2018

Material Characteristics of Binder Jet 3D Printed Hydrated CSA Cement and Fine Aggregates

Joseph P. Ingaglio
Lehigh University, josephingaglio@gmail.com

Material Characteristics of Binder Jet 3D Printed Hydrated CSA Cement and Fine Aggregates

by

Joseph P. Ingaglio

A Thesis

Presented to the Graduate and Research Committee

of Lehigh University

in Candidacy for the Degree of

Master of Science

in

Structural Engineering

Lehigh University

August 2018

This thesis is accepted and approved in partial fulfillment of the requirements for the Master of Science.

_____
Date

_____
Clay J. Naito
Thesis Advisor

_____
John T. Fox
Thesis Co-Advisor

_____
Paolo Bocchini
Thesis Co-Advisor

_____
Panayiotis Diplas
Chairperson of Department
Civil and Environmental Engineering

ACKNOWLEDGEMENTS

The author would like to thank Buzzi-Unicem USA of Bethlehem, PA for their generous support and material donations. This project was also financed in part by a grant from the Commonwealth of Pennsylvania, Department of Community and Economic Development, through the Pennsylvania Infrastructure Technology Alliance (PITA). This work was also supported in part by Lehigh University's Mountaintop Initiative, through the office of Creative Inquiry.

A special thanks to the following undergraduates and graduate student researchers who assisted with the research efforts: Kyle Root, Matt Gombeda, Nicholas D'Angelo, Ian Black, Andrew Novillo, Connor Bradley, Greg Casee, Jessica Lloyd, Theresa Colonna, and Matt Montano.

The author would also like to recognize his Parents, Raphael and Lisa Ingaglio, and his fiancée Abby Winter, for their continued support throughout his academic years.

Lastly, the author would like to acknowledge his three advisors, Dr. Clay Naito, Dr. John Fox and Dr. Paolo Bocchini, for their guidance throughout his studies.

TABLE OF CONTENTS

LIST OF TABLES

LIST OF FIGURES

ABSTRACT

Recent advances in additive manufacturing technologies for concrete construction have been limited to low resolution fused deposition methods, herein the author aims to advance high resolution binder jet printing methods for cement construction applications. The inherent challenge of additive binder jet cement printing is to achieve adequate mechanical strengths and maintain geometry without the agitation typical of conventional concrete fabrication. The author utilizes a commercially available binder jet printer to fabricate sample specimen objects that are utilized to assess material and geometric properties. A novel water based jettable binder formulation, compatible with concrete chemistry, is developed. This study examines a dry cementitious powder mix comprised of round grain fine aggregates and CSA cement. The printed samples have a density of 1474 to 1501 kg/m^3, 28-day compressive strengths of 5.94 to 6.70 MPa, and tensile strengths of 0.85 to 1.22 MPa. The results indicate that printed CSA cement objects possess the strength and the resolution to produce high detail objects that offer rapid production capability and compatibility in applications with conventional construction materials.

1. INTRODUCTION

In recent years, additive manufacturing of cement-based materials has been at the forefront of construction technologies as it allows direct conversion from digital design to build [1]–[8]. One of the most attractive capabilities of additive manufacturing is that it enables greater design freedoms than conventional techniques [9]. Relative to conventional cast cementitious materials the elimination of formwork can eliminate up to a 60% of costs when compared to a typical concrete structure [10]. Multiple 3D printing methods have been developed including stereo lithography, liquid binder printing (3DP), selective laser sinter or melting, fused deposition modeling (FDM), digital light processing, and others. Of these methods the two which lend themselves to 3D printing of concrete products are 3DP and FDM. In general, 3DP can be considered a dry method and FDM a wet method. In simple terms 3DP consists of a dry powder bed which is sprayed with a liquid binder, whereas FDM consists of direct deposition of a flowable material. There are commercially available FDM systems and FDM-like systems that are capable of printing large scale cement structures, such as small houses, wall panels, and structural elements and have evolved from initial devolvement of counter crafting initiated by Khoshnevis [5], [11].

In FDM, layers are comprised of extruded premixed zero slump concrete made with fine aggregates (Figure 1a). The premixed material is mechanically extruded in layers typically ranging from 1 to 10 cm in thickness. The extrusion process is repeated vertically, with one layer printed on top of another, until the desired object is formed. Due to the nature of FDM, each layer must be supported by the previously printed layer or the printing must be interrupted to allow manual installation of supports and/or formwork. This deposition technique inherent to FDM precludes certain geometric features such as

overhangs, large openings, and internal voids and is best suited for simple components like solid vertical walls. In addition, due to the relativity large layers and slumping of the concrete, the surface quality of the finished product is often rippled and poor bond between subsequent layers lowers the already low tensile properties of concrete. FDM concrete printing can be effective for large robust components where surface quality and accuracy are not critical. However, concrete FDM is not suitable when complex geometries, refined topologies, lightweight components and architectural details, the most appealing aspects of architectural and structural 3D printing, are desired. The drawbacks of concrete FDM printing are thoroughly discussed in work published by Bos [12] and Feng [13].

In an effort to overcome the shortcomings of FDM, the author utilizes a 3DP method to spray a water-based cement compatible liquid binder onto a blend of dry CSA cement powder and fine round grain silica aggregate (Figure 1b-d). This approach facilitates the fabrication of more complex components, as the printed objects are fully supported during construction by the unsaturated powder material. Further, 3DP allows for complex shapes such as negative draft, hollowed sections, direct fabrication of topology optimized objects, and a limitless array of surface details that are not currently possible with fabricated formwork and/or FDM construction techniques. In most 3DP applications the dry material is bonded via adhesives supplied by the binder, but in this study it was preferred to leverage the bonding provided by hydrated cement, with which the construction industry is much more familiar, in terms fabrication, life-cycle properties, management, and decommissioning. Hence, when performing cement 3DP, a water-based binder can be deposited onto cementitious materials and enable the hydration process to bind the materials together [14]. This hydration process must occur rapidly, in order to

minimize the bleeding of excess water, maintain shape while printing, and achieve the early strength needed for removal of the object from the print bed.

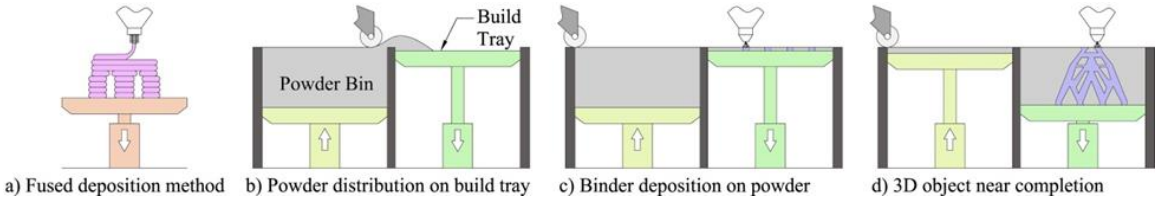

Figure 1: FDM printing (a) vs Binder Jet Printing (b-d)

Previous work by Shakor was performed using ordinary Portland cement (OPC), Calcium aluminate cement (CAC), fine aggregates, and a proprietary (Z Corporation) binder [15]. Based on the composition of the proprietary binder, limited hydration occurred in the work by Shakor. For the work herein, the author performed preliminary work with Portland cement, and other varieties of cementitious materials combined with water-based binders. Based on these preliminary results the study herein focused on CSA type cement due to the hydration properties and rapid strength gain. CSA, or calcium sulphoaluminate cement ($Ca_4(AlO_2)_6SO_4$ or C_4A_3S), was originally developed by the China Building Materials Academy in the 1970's [16]. The early stages of hydration for CSA are much more rapid than conventional Portland cement, with ettringite formation initiating in as little as 5 minutes [17]. This rapid reaction can have a negative effect on workability for conventionally fabricated concrete, but is ideal for 3DP in order to reduce bleeding and distortion of the printer specimens. Within 3DP applications, Portland cements require too long to hydrate and result in large printing errors due to the bleeding of the binder. For conventional applications most Portland cement is mixed with other products to increase workability, whereas for printing applications workability is not a concern. Both ASTM C150 Type I and III cements were initially investigated. Type III is utilized for high early

strength applications and is capable of rapid strength gain. Type III provided marginal improvements over type I; however, the conventional 50 mm compression cube specimens manufactured with both mixes were too distorted to be accurately measured and tested. Therefore Type I and III cements were abandoned in favor of CSA cement. In addition to its more favorable printing properties, CSA cement is innately more sustainable than its Portland cement counterpart. The manufacturing process of CSA clinker requires lower temperatures and considerably less limestone, so allowing the produced CSA to expend approximately half the amount of CO2 required by Portland clinker [17].

In order to utilize 3D printing components in structural or architectural applications it is necessary to perform a through material characterization. As such, the following discussion will demonstrate the first work of a 3DP system utilizing hydrated CSA cementitious materials. Feng proposes that conventional assumptions and theories of traditional concrete need to be redeveloped in order for the 3DP technology to become practical [13]. The author provided initial assessments of the physical and mechanical properties of the material specimens printed with this novel process and printed specimens, including; 28-day compressive strength, flexural strength, tensile strength, elastic modulus, density, and total voids.

2. MATERIALS AND METHODS

2.1. 3D Printer

A commercially available binder jet printer was utilized for the fabrication. A Zcorp 310+ printer produced by the Z Corporation (now part of 3D Systems of Rock Hill, SC) was acquired to jet liquid adhesive binders onto dry powders. The printer utilizes disposable HP10 piezoelectric ink print heads, allowing for simple and cost-effective

printing, which is especially important during material research and development. The HP10 print head provides print good print accuracy, with a resolution up to 300 x 450 dpi. The printer has a print bed that is 20.3 cm long, 24.4 cm wide, and 20.3 cm deep. The ZCorp 310+ is capable of printing layers from 76.2 μm to 254 μm thick, at a rate of approximately 3 layers per minute. The printer defines the horizontal print bed as x and y axis, whereas the vertical direction from layer to layer is the z axis. As with the majority of 3D printing systems, the stereolithography (STL) file format is used to describe the geometry of the object. The 3DP platform provided by the ZCorp 310+ allows for seamless scale-up to commercially available printers with larger build trays that function similarly. For instance, ExOne (North Huntingdon, Pennsylvania) currently produces similar 3DP printers with nearly 3.7 cubic meters of build volume [18].

2.2. Binder

A water based liquid binder was formulated, because cement materials require water in order to perform the critical hydration process, as such organic solvents are not suitable for cement 3DP. Further, piezoelectric print heads require that in order for a binder to be Jettable it must maintain a specific relationship between viscosity and surface tension. The HP10 cartridges used by the Zcorp printer piezoelectric print heads require a surface tension of approximately 45 dyn/cm and a viscosity of approximately 1.35 cP [19]. Preliminary tests were performed by the author with pure water, but this jetted poorly through the HP10 print head as the surface tension was too high (72 dyn/cm) and the viscosity too low (1.00 cP). The novel water based binder was formulated with the intent to obtain these desired physical properties and it includes a water soluble polymer and a

surfactant. This binder was extensively tested with multiple types of cement, beyond CSA, and was found compatible with all the tested cement types.

2.3. Dry mix

The dry powder mix was comprised of a silica sand and CSA cement, which is blended by hand and loaded into the powder print bed. Preliminary work investigated several types of fine aggregates that could be evenly dispersed by the printer's spreading mechanism. The Zcorp uses a roller bar to evenly spread out the dry material and is very sensitive to particle size and shape. A smooth build bed is required in order for the printer to function accurately and avoid print error. A round grain Wedron Silica 730 sand was selected and provided by Lancaster Foundry Supply (Lancaster, PA). This fine aggregate, when mixed with the CSA cement, consistently produced smooth and evenly distributed print beds.

Table 1: Wedron Silica 730 Sand Gradation [20]

Mesh Size [µm	US Mesh Size	Percent Retained
600	30	0.0
425	40	0.0
300	50	2.2
212	70	14.7
150	100	47.5
106	140	28.8
75	200	6.4
53	270	0.4
<53	PAN	0.0

This fine round grain silica sand has approximately 97.8% pass through a US Mesh 50 sieve (300 μm) (

Table 1). This relativity small particle sizes allows for even distribution and high print accuracy. In addition, the silica sand is a natural round grain, which facilitates its even spreading. The Wedron Sand is cleaned so that there is no sand particles that are retained below a US Mesh 270 sieve (53 μm). This "dust" could hinder binding and ccould absorb excess water away from the hydration reaction [21]. Since the amount of liquid added to the mix will be held to a minimum, additional absorption of water is not ideal. The Wedron sand was tested according to ASTM C128 and was found to have an absorption of approximately 2.3% by mass [22]. This value is used in the calculation of the water to cement ratios of the mixes.

2.4. Mix Design

Mix designs were developed based on the properties and requirements of the ZCorp printer and from preliminary trials performed by the author. Due to the nature of 3DP and the printer, the amount of liquid that can be applied via binder jetting is limited, becuase excessive binder applied to the powder bed would cause the printed object to "bleed", which means that the binder moves beyond the defined geometry and the desired shape is lost. Due to this, the water to cement ratio (w/c) is relatively low compared to conventionally mixed concrete designs. Herein, the author appraises two test mixes. The water to cement (w/c) ratio was designed to be 0.293 (Mix A) and 0.373 (Mix B), but due to the 2.3% absorption and 0.1% moisture content of the sand, the w/c ratio in hydration is reduced to 0.221 and 0.301, respectively. The actual w/c ratio may be lower, because this

study did not account for water loss due to bleeding into the surrounding particles or evaporation.

From preliminary testing, the author determined a sand to cement ratio, based on the amount of cement needed to adequately bind the relative high surface area of the fine aggregates. The amount of water was set to the maximum value of the printer and a set of three ATSM cubes were molded and tested in compression at 7 days (Table 2). During preliminary testing the sand to cement mass ratio was varied from 1.25:1.00 to 5.05:1.00. The ratio of 1.25:1.00 resulted in a w/c ratio of 0.197, which was too low for proper hydration to occur, whereas increasing the ratio to 5.05:1.00 (0.559 w/c) resulted in not enough cement content to adequately adhere the large amount of fine aggregate. The author determined that an optimal sand to cement mass ratio was 3.20:1.00. This allowed the sand to adequately bind and achieve hydration of the cement and produced the highest tested strengths. The author formulated two distinct compositions using this ratio. The first mix (Mix A) used a reduced amount of water, whereas the second mix (Mix B) used the maximum amount of binder the printer could deposit. The initial intent of the mix designs was to have a more accurate, but possible weaker mix A and more hydrated and stronger Mix B, with less print accuracy. The composition of each mix is listed in Table 3.

Table 2: Mix Design Sand/Cement Ratio Preliminary Testing

Sand:Cement Mass Ratio	Design w/c Ratio	7 Day Avg. Comp. Strength [MPa]
5.05:1.00	0.559	10.76
3.20:1.00	0.373	13.38
2.20:1.00	0.291	10.14
1.25:1.00	0.197	8.48

Table 3: Mix Design Parameters Presented by Mass

Mix	CSA Cement [kg] (S.G)	Wendron 730 Sand [kg] (S.G.)	Binder [kg] (S.G.)	Design Unit Weight [kg/m^3]	Design w/c Ratio	Actual w/c Ratio
Mix A	1.00 (3.15)	3.20 (2.65)	0.293 (1.01)	2474	0.293	0.221
Mix B	1.00 (3.15)	3.20 (2.65)	0.373 (1.01)	2414	0.373	0.301

2.5. Specimen Fabrication Process

The process of printing a sample object with the ZCorp printer begins by creating an object in standard triangle language (STL) file format. The STL file is then read and sliced into print layers using the Zcorp, ZPrint software. Using the Zcorp interface, parameters such as layer thickness and binder deposition level can be modified.

In order to begin a print, the author loads the specific dry mix powder into the feed tray, and the printer automatically levels the build tray before printing. Next, the formulated water based liquid binder is loaded into the binder reservoir, which subsequently feeds the print head. Once the printing process is started, the 310+ printing moves at approximately 3 vertical centimeter per hour, but the speed can vary depending on the amount of binder being deposited, layer thickness, and cross-sectional area of the printed object. For example, for two layers of 50 mm cubes (6 per layer, 12 total), the print time is approximately 4 hours. After the printing is complete, samples are allowed to cure in the powder bed for approximately 24 hours. This allows the initial hydration reaction to occur and prevents damage during removal. The objects are then removed from the build tray, where any loose powder that the binder did not contact, falls away and remains in the printer. The printed objects are then transferred to a removal chamber for cleaning with a bristle brush, compressed air, and a vacuum. This cleaning process can take up to several

minutes for more complex printed objects. After the test specimens are cleaned, there mass and size are measured before being placed in a water bath. The test specimens were submerged and continued to hydrate until the desired testing day (e.g. 28 days).

Control specimens were produced by conventionally mixing the CSA cement, water, and aggregate and forming samples. Specifically, the materials were weighed and mixed together in a ASTM compliment mixer for approximately 2 minutes at 139 RPMs, and were then packed into molds by hand. After 24 hours of air curing, the control samples were removed from the mold, weighed, measured and placed in the water bath with their printed counterparts until the desired testing date. Due to the fast-acting nature of the CSA cement (without retarders), molded control samples were difficult to pack and had to be completed in matter of minutes. In addition, the relative dryness of the mix caused poor workability, and high levels of compaction were not feasible (in the control samples).

2.6. Printing Tolerance and Density

During the printing process, fabrication errors can occur. For 3DP the most common error is bleed, where the jetted liquid blinder is absorbed by surrounding dry areas. Bleed can occur in all three build planes (x, y and z). The amount of bleed relative to the specimen sizes decreases as the printed dimensions increase and is typically consistent throughout all build layers (x axis and y axis). For the z axis, the bleed is mostly from the bottom most layers, but bleeding upwards can occur. Bleed can also vary due to the mix design and the amount of water based binder applied. Sets of various rectangular prisms were created in addition to the strength testing specimens to determine the printing resolution of the system at various print sizes. The samples ranged in size from 13 mm to 152 mm and were arranged so that the bleed in all 3 planes of geometry could be measured. The lack on compaction

in addition to the bleed can cause the density of the printed objects to be relatively low. Comparison of the design unit weight and specimen density allow for percent voids calculation.

2.7. Compression Testing

Ultimate compressive strength was determined for both mix designs by fabricating 50 mm ASTM C109 compression cubes through printing and conventional mixing. The compression cubes were tested at intervals of 24 hours, 7 days and 28 days from time of printing completion, with the appropriate testing parameters [23]. There were a total of four trials completed, which included: 3D Printed Mix A, 3D Printed Mix B, Molded Mix A (conventional control), and Molded Mix B (conventional control). The printed specimens were appraised in two different orientations, the first with the loading normal to the print layers (Normal Stress) and the second with the loading parallel to the print layers (Parallel Stress). Testing with respect to orientation was performed to ascertain if the printer layer orientation caused the material to be anisotropic. A scheme of the print orientations with the respect to the applied loading is shown in Figure 2.

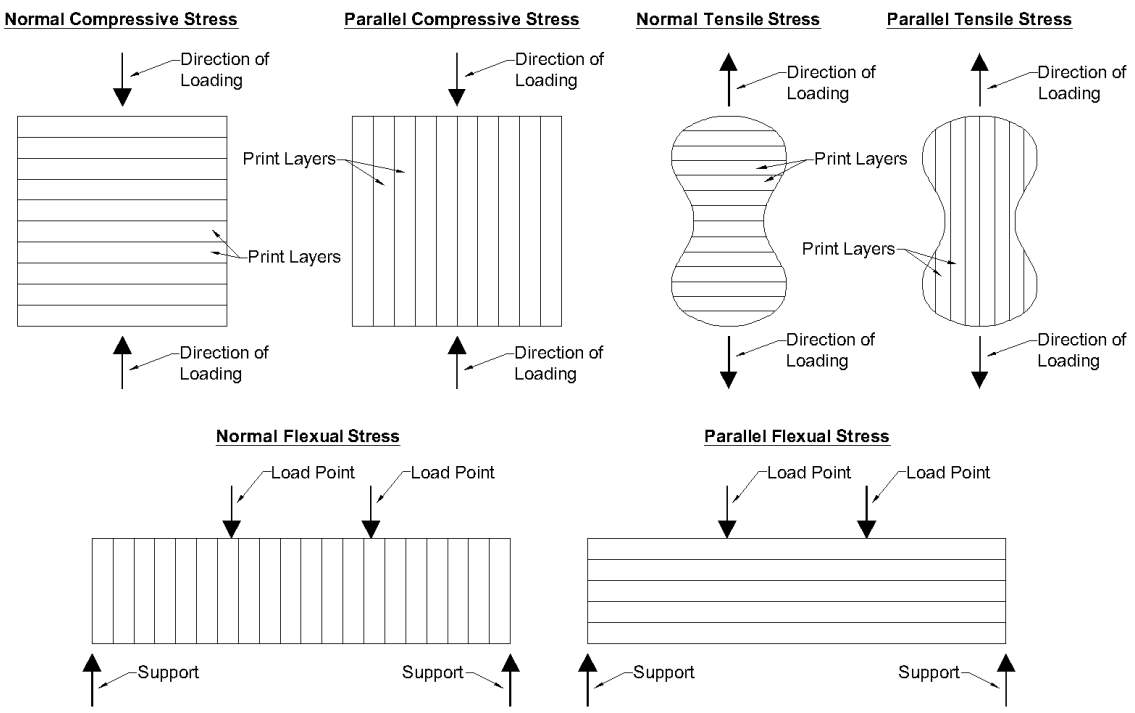

Figure 2: Printed Specimens Loading Orientations

2.8. Flexural Testing

Beam prism specimens were fabricated at one quarter scale, 38 mm x 38 mm x 152 mm, and were tested in third-point bending according to ASTM C78 to determine flexure strength [24]. All samples were tested at 28 days from time of fabrication. The same 4 trials preformed for compression were done also for flexural testing. The printed prisms were fabricated in two directions: a vertical orientation was used so that the applied bending stresses would be normal to the print layers, a horizontal orientation was used so that the bending stresses would be parallel to the print layers (Figure 2). The molded control prisms were produced with formwork and did not have an orientation associated with their fabrication.

2.9. Tensile Testing

Tensile testing was performed using AFS Test Procedure 3301-00-S, as per the AFS Mold and Core Test Handbook [25]. In foundries, it is common practice to routinely measure the tensile strength as a quality control of chemically bonded sands, which are used to make complex mold and core geometries. This procedure requires test specimens with a 25 mm x 25 mm cross section and a curved profile similar to a "dog bone". These tensile specimen samples were tested at 28 days from time of fabrication. The four standard trials were conducted. Similar to the printing method of the prisms, the dog bones were printed in two orientations (Figure 2). The first dog bone set was printed with the specimens oriented vertically in the build, so that the tensile stresses would be normal to the print layers. The second dog bone set was printed horizontally, so that the tensile stresses would be parallel to the print layers. The molded dog bones were fabricated in brass molds and did not have an orientation associated with their construction.

2.10. Elastic Modulus

To measure the compressive modulus of elasticity of the printed samples, a set of cubes were tested in compression using an Instron 5500 testing machine (Instron, Norwood, MA). The testing setup was equipped with a digital image correlation camera and software that measures the displacement of two painted marks on the surface of the cube. The software then calculates the displaced distance between the two points to determine the strain in the specimen relative to the applied load. In this way a stress/strain relationship can be determined, which can then be used to derive the elastic modulus. This measured elastic modulus can then be compared to ACI 318 equation (Eq. 1), which correlates elastic

modulus (E_c) to the unit weight (w_c) and the ultimate compression strength of the concrete (f'_c) [26].

$$E_c = 0.043 w_c^{1.5} \sqrt{f_c'} \, [MPa] \quad \text{(Eq. 1)}$$

2.11. Curing

Following fabrication, and 24 hours of undisturbed curing in the print bed or molded formwork, all samples were water cured. Once samples were removed from the print bed and cleaned, samples were placed in a room temperature water bath until testing at either 7 days or 28 days. For samples tested at 24 hours, no curing was performed. Due to the limited water that is applied to the mix during fabrication and the lack of mixing, the water bath enables unhydrated or under-hydrated cement to access to water and hydrate. The samples are porous enough to allow a water infiltration through the section during water curing.

2.12. Specimens

This study consisted of 84 tested specimens, 54 printed and 30 molded. Examples of the printed and molded specimens are shown in Figure 3. The test matrix for the printed and molded specimens is reported in Table 4.

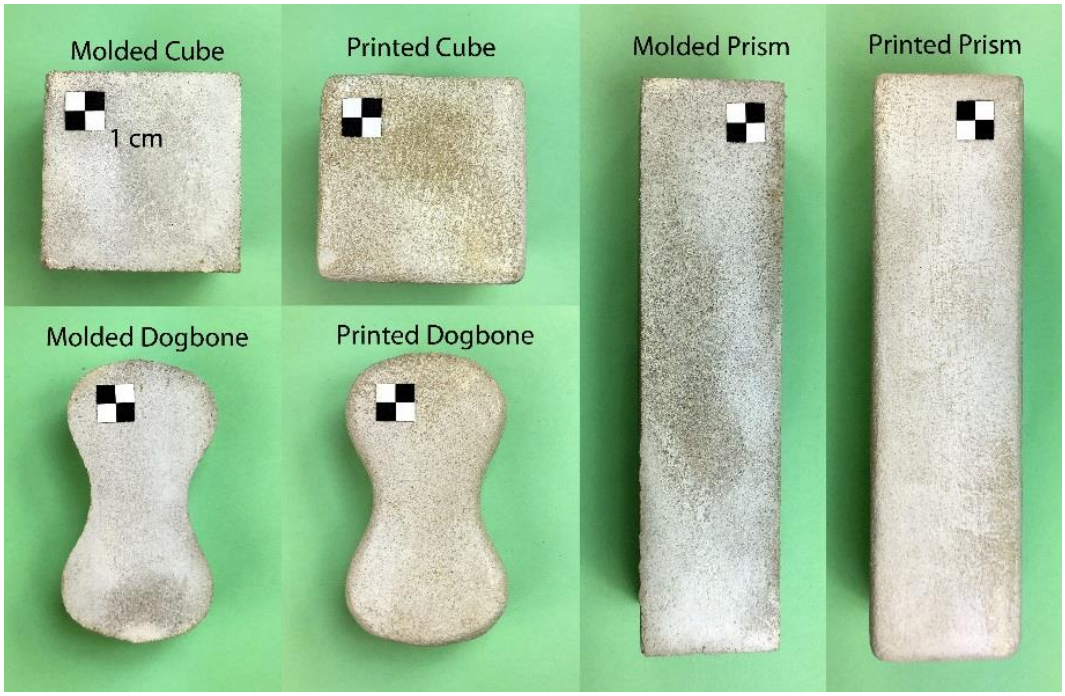

Figure 3: Printed and Molded Test Specimens

Table 4: Specimen Test Matrix

Mix Type	Specimen Type	Quantity Printed/Molded	Age Tested	Property Tested
Mix A	Cubes	3/3	24 hours	Compression
Mix A	Cubes	3/3	7 Days	Compression
Mix A	Cubes	6/3	28 Days	Compression both orientations
Mix B	Cubes	3/3	24 hours	Compression
Mix B	Cubes	3/3	7 Days	Compression
Mix B	Cubes	6/3	28 Days	Compression both orientations
Mix A	Prisms	6/3	28 Days	Flexure both orientations
Mix A	Dog	6/3	28 Days	Tension both orientations
Mix B	Prisms	6/3	28 Days	Flexure both orientations
Mix B	Dog	6/3	28 Days	Tension both orientations
Mix A	Cubes	6/0	28 Days	Elastic Modulus

3. EXPERIMENTAL RESULTS

3.1. Printing Tolerance and Object Density

One innate property of 3DP materials is the low density, which is an artifact of the layered production of a liquid bound component on a dry powder bed. The low density enables the specimen to receive further processing such as sintering or infiltration to increase density [19]. This low density is primarily due to the lack of compaction and consolidation in the loose powder bed. Several commercial 3DP methods utilize post treatment of printed specimens with infiltration of a liquid wax or glue to provide additional reinforcement. The liquid penetrates and fills all the unwanted voids, which increases the density and strength of the printed objects. Another alternative is to use a source of heat to sinter adjacent particles; this is most common in metal powder printers. For the concrete study conducted herein, no post processing was performed.

The print accuracy was examined through the measurement of the geometry following removal from the print bed. The print head has a relatively high resolution (300 x 450 dpi), thus any measurable error in print accuracy is a function of the amount of bleed that the printed component experiences during the fabrication. A series of print specimen with increasing size were fabricated. Mix A varied from 21.8% to 4.3% in the x and y planes and 20.0% to 4.8% for the z plane (Figure 4). For larger print objects the dimensional errors in the printed components are less than 5%. Note that the errors are measured immediately after objects are removed from the printer and do not include any finishing. If a more accurate shape is desired, the object can be lightly tooled down to the exact printed dimension before the cement is fully hydrated. This allows the user to achieve as little as 0% error with minimal effort.

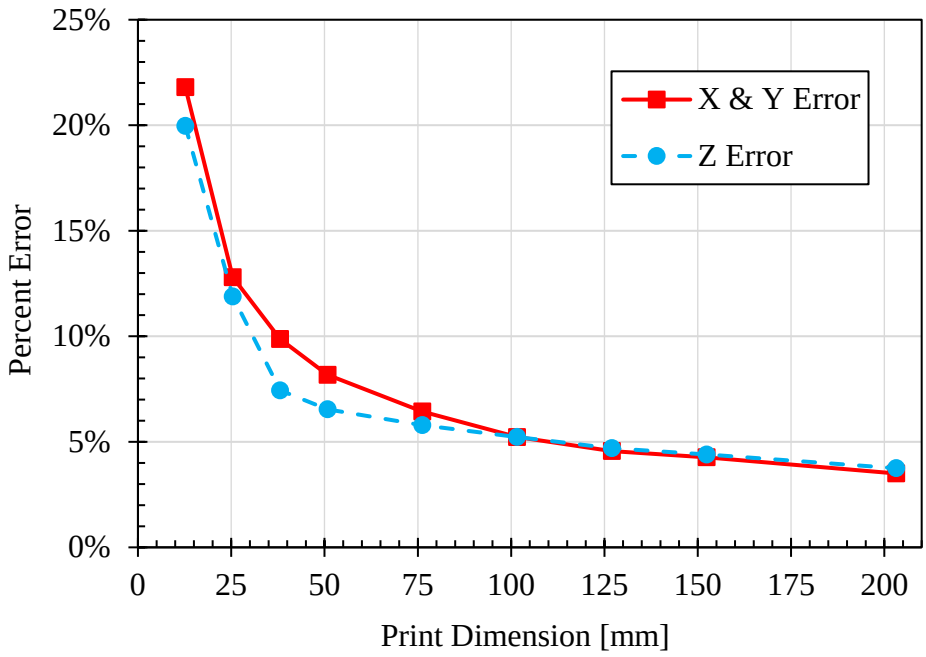

Figure 4: Printer Bleed Correlation with Print Dimension

The unit weights of the specimens were determined after printing to assess the amount of air voids present. For Mix A, the theoretical maximum unit weight is 2474 kg/m^3 and for Mix B it is 2414 kg/m^3 (Table 3). These unit weights are approximated assuming that voids are 0% and that the only water lost in the hydration reaction is due to the absorption of the sand. The printed specimens were weighed and measured, and the fabricated density calculated. The amount of air voids present was determined by taking the differences of the theoretical maximum density and the constructed density and dividing by the theoretical maximum density. The majority of the voids are microscopic, as they cannot be seen on the surface.

The printed samples in this study had lower density and higher voids, than the conventional samples, which was expected for the reason explained previously (lack of mixing and compaction). Mix A printed specimens averaged 1474 kg/m^3, which corresponds to 40.4% voids (Table 5). Mix B printed specimens had an average density of

1501 kg/m^3 and 37.8% voids (Table 5). The conventionally molded specimens had higher density due to the mixing and compaction that were applied during packing of the molds. Mix A molded density averaged 1704 kg/m^3 and Mix B averaged 1826 kg/m^3 which corresponds to a 31.1% and 24.3% voids, respectively. During the printing process the specimens increased their air content by 9.3% and 13.5% for Mix A and B, respectively.

Table 5: Cube Densities and Voids

Mix Design	Density (kg/m^3)	Calculated Air Content
Printed Mix A	1474	40.4 %
Printed Mix B	1501	37.8 %
Molded Mix A	1704	31.1 %
Molded Mix B	1826	24.3 %

Note: All Measurements are at time of removal, ~24 hours after completion.

3.2. Compressive Strength

Standard 50 mm cube specimens were tested in compression at 28 days. The printed cube specimens were loaded both normal to the printed layers and parallel to the printed layers. Under normal loading, the stresses propagates perpendicularly to each layer as layers are compressed together. The normal loaded printed specimens possessed a compression strength of 6.29 MPa for Mix A and 5.94 MPa for Mix B (Table 6). Mix B had been design to have higher compression strength, due to its higher density and better hydration. However, it was characterized by slightly worse compression strength. This lower strength could likely be due to the excessive bleed associated with larger amount of water deposited by the printer. The excessive bleed caused the cubes to become larger than anticipated and thus a larger cross-sectional area is used during strength calculations. For the cases with parallel orientation of layers and loads the results were similar to those with normal loading, with Mix B at 5.94 MPa and 6.70

MPa for Mix A. Conventionally molded specimens achieved higher compressive strength than their printed counterparts, with Mix A achieving 11.93 MPa and Mix B achieving 15.73 (Table 6). This higher strength of Mix B over Mix A, is likely due to better hydration of Mix B and better packing of the mold, as more water provided a more workable mix.

Table 6: Cube Compressive Strength

Mix Design (Stress Orientation)	Compressive Strength (MPa)	Standard Deviation (MPa)
Printed Mix A	6.29	±0.90
Printed Mix A	6.70	±0.63
Printed Mix B	5.94	±0.70
Printed Mix B	5.94	±0.58
Molded Mix A	11.93	±1.30
Molded Mix B	15.73	±0.60

Note: All Measurements are at 28 days.

In addition to 28 day compressive strength, the specimens were also tested at 24 hours and 7 days to establish a strength gain curve. The specimens that were tested at 24 hours were not cured at all and were tested directly after removing them from the printer or molds. The 7-day testing specimens were water cured and removed 2 hours prior to testing. Typical CSA cement achieved high early strengths, but for both printed mixes and for molded specimens made of Mix A, the majority of the strength gain occurred between 24 hours to 7 days (

Figure 5). On the contrary for molded specimens made of Mix B, the majority of the strength gain was in the first 24 hours, which is typical for standard CSA cement mix designs. This is the results of the fact that both printed mixes and the drier Mix A have too little initial water in their mixes to properly hydrate, so when placed in the water bath at 24

hours, the CSA cement absorbs the excess water and continues to hydrate more than a typical mix design would. This was also verified when Mix A and Mix B printed specimens achieved similar strengths at 7 and 28 days. The strength gains of all specimens were inputted into the ACI 209R equation (Eq.2), and the constants, alpha and beta were computed [27].

$$(f'c)_t = \frac{t}{\alpha+\beta t}(f'c)_{28}[MPa] \text{ (Eq. 2)}$$

Where $(f'c)_t$ is the compressive strength at t time and $(f'c)_{28}$ is the compressive strength as 28 days. For the CSA cement and the described curing conditions, alpha was found to be 3.15 whereas beta was 0.827. These values can be used to predict the strength of the specimens and they correlate well with the experimental data even through in all 4 cases the equation slightly over predicted the strength at 28 days. The amount of water applied during the printing has little effect on the final strength of the specimens. This allows for a lower amount of water to be placed during printing, and a more accurate and faster printing is possible.

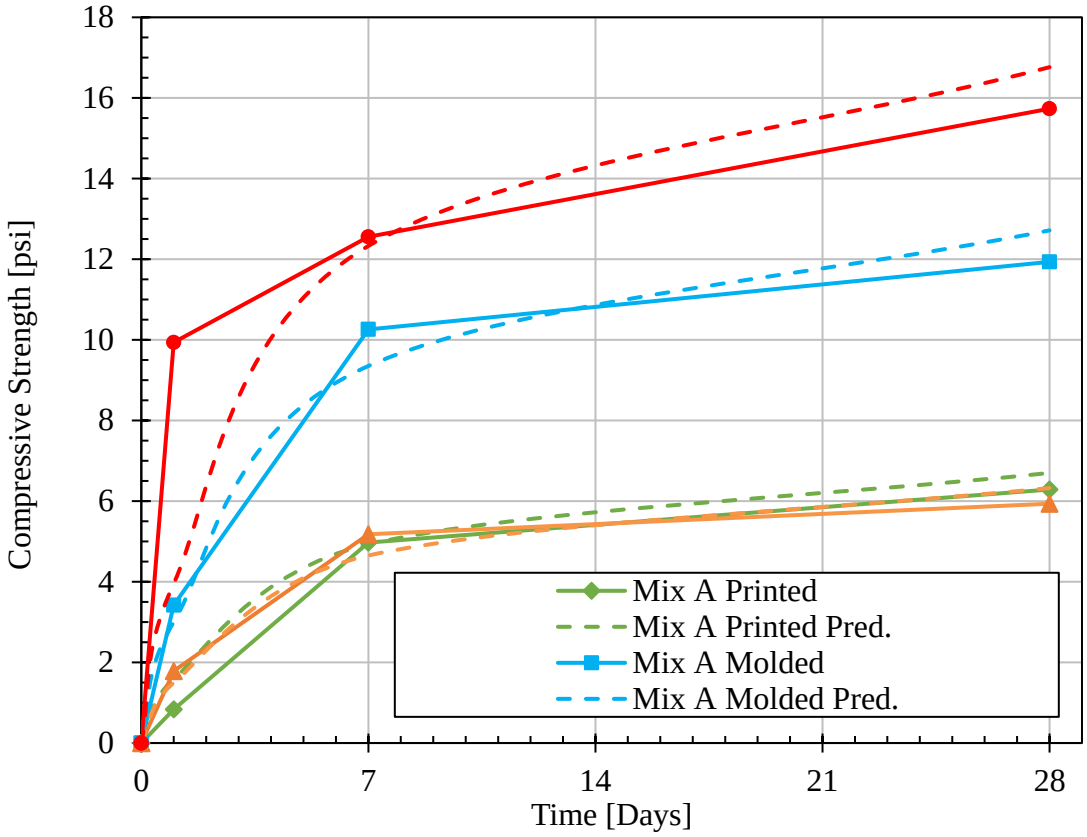

Figure 5: Compressive Strength Gain & ACI209 Predicted Gain (Alpha=3.15 & Beta=0.827)

3.3. Flexural Strength

Flexural loading of concrete often fails in tension, but the quantified flexural strength value is often higher than the direct tensile strength value. This larger strength is due to the combination of compression and tension forces through the flexural member. Both the printed and molded specimens were tested at a one quarter scale compared to the ASTM C78 Beam test. This ASTM test utilizes four-point bending to create a constant moment through the middle third of the beam. All tested prism specimens failed in tension, however the prisms with print layers in normal orientation failed at slightly lower values than those with parallel orientation. As reported in Table 7, the normal orientation prism failed at 1.89

MPa and 1.76 MPa, respectively for Mix A and Mix B, whereas, the prism specimens tested in parallel orientation to print layers failed at 2.32 MPa for Mix A and 2.39 MPa for Mix B.

The lower flexural strength values of the printed samples tested in the parallel orientation is due to the imperfect bonding between sequential layers of the printed specimens. As the strength of each layer is greater than the strength between layers, when the applied stresses occur in the normal orientation the resultant forces are pulling the layers apart, and the specimens fail when the layers deboned from the adjacent layer. These results were expected for both mixes, this behavior needs to be considered in design and application of 3DP cement materials, as the differences in directional flexural strength was reduced by 18.7% for Mix A and 26.3 % for Mix B. Since, the molded specimens did not have a build orientation, only one direction was tested. Flexural strengths are reported in Table 7 and were calculated to be 3.08 MPa and 3.86 MPa for Mix A and Mix B, respectively.

Table 7: Prism Flexural Strength

Mix Design (Stress Orientation)	Flexural Strength (MPa)	Standard Deviation (MPa)
Printed Mix A (Normal)	1.89	±0.16
Printed Mix A (Parallel)	2.32	±0.09
Printed Mix B (Normal)	1.76	±0.04
Printed Mix B (Parallel)	2.39	±0.13
Molded Mix A	3.08	±0.83
Molded Mix B	3.86	±0.20

Note: All Measurements are at 28 days.

3.4. Tensile Strength

Cementitious based materials possess an inherent lack of tensile strength, which is why reinforcement is common. The poor tensile strength of cementitious materials is due to the

inability of the concrete bonds to yield in place of cracking. The tensile strength was tested in both normal and parallel orientations to the print layers, and a lower strength for the normal orientation of printed mix designs was found. As reported in Table 8, Mix A achieved 0.85 MPa in case of normal orientation and 1.17 MPa with parallel orientation. Mix B performed similarly, with strengths of 0.86 MPa and 1.22 MPa, respectively for normal and parallel orientations. When printed samples were placed under tension, the normal case failed earlier due to the layers being pulled apart, which occurred due to the lowered strength between sequential printed layers than within the layers. The molded specimen achieved higher tensile strengths than the printed materials, with tensile strengths of 1.77 MPa for Mix A and 2.10 MPa for mix B.

Table 8: Dogbone Tensile Strength

Mix Design (Stress Orientation)	Tensile Strength (MPa)	Standard Deviation (MPa)
Printed Mix A (Normal)	0.85	±0.03
Printed Mix A (Parallel)	1.17	±0.14
Printed Mix B (Normal)	0.86	±0.06
Printed Mix B (Parallel)	1.22	±0.13
Molded Mix A	1.77	±0.17
Molded Mix B	2.10	±0.39

Note: All Measurements are at 28 days.

3.5. Elastic Modulus

Six printed specimens were tested for elastic modulus, in order to quantify the stiffness of the 3DP samples. The author used a digital image correlation camera to assess the strain under applied load onto 50 mm cubes with a gage length of 25 mm. The samples exhibited elastic moduli generally higher than those predicted by the ACI 318 equation [26]. The average of the three tested specimens was 7705 MPa. More specifically, the experimentally

measured modulus was approximately 21.5% higher on average than the one calculated for the three cases.

Table 9: Experimental Elastic Modulus Compared to Calculated Modulus

Sample	Compressive Strength (MPa)	Density (kg/m^3)	ACI 318 Modulus (MPa)	Measured Modulus (MPa)
Mix A-1	6.96	1462	6310	7252
Mix A-2	6.00	1479	5948	7428
Mix A-3	7.80	1475	6759	8435

3.6. Printing of Complex Geometrics

The printer system is capable of fabricating complex geometries. As a demonstration, am intricate component was printed which includes openings and voids which would not be obtainable using conventional concrete fabrication approaches, such as formwork or other techniques such as mold making or FDM concrete printing methods. The specimen consists of eight complex curved and sweeping columns that intersect one another. The specimen also contains several openings and voids through the center, as well as rounded protrusions and cavities on the top face. This specimen is approximately 152 mm x 152 mm across and 170mm tall. The specimen was created in one print and took approximately 4 hours to produce (

Figure 6). This specimen is only a sample of what the 3DP method can produce, as more complex features are easily obtainable.

Figure 6: Geometric Sample Print, Front View (Left), Side View (Center), STL (Right)

4. CONCLUSIONS

The results indicate that 3D printed hydrated CSA cement objects possess the strength and the resolution need to fully utilize the advantages of additive manufacturing. By virtue of these 3DP methods, the printed CSA cement objects can be printed with more detail, higher resolution, and more geometric freedom than current FDM concrete printing. The benefit of utilizing a cement based material, is that compatibility of applications it possess and how easily it can be integrated with conventional construction materials in the construction industry. The performance of 3DP CSA cement mixes are typical of other conventional lower strength cementitious mixes and anisotropic behavior is present but is minimal. The author is aware that the current strength may be too low for structural applications, and would most likely need to be improved in order to be used in a structural capacity. The author also believes that a compressive strengths of 25 MPa or greater is obtainable with this 3DP method in the near future.

5. REFERENCES

[1] I. Hager, A. Golonka, and R. Putanowicz, “3D Printing of Buildings and Building

Components as the Future of Sustainable Construction?," *Procedia Eng.*, vol. 151, pp. 292–299, Jan. 2016.
[2] A. Perrot, D. Rangeard, and A. Pierre, "Structural built-up of cement-based materials used for 3D-printing extrusion techniques," *Mater. Struct.*, vol. 49, no. 4, pp. 1213–1220, Apr. 2016.
[3] K. Henke and S. Treml, "Wood based bulk material in 3D printing processes for applications in construction," *Eur. J. Wood Wood Prod.*, vol. 71, no. 1, pp. 139–141, Jan. 2013.
[4] G. Cesaretti, E. Dini, X. De Kestelier, V. Colla, and L. Pambaguian, "Building components for an outpost on the Lunar soil by means of a novel 3D printing technology," *Acta Astronaut.*, vol. 93, pp. 430–450, Jan. 2014.
[5] C. Gosselin, R. Duballet, P. Roux, N. Gaudillière, J. Dirrenberger, and P. Morel, "Large-scale 3D printing of ultra-high performance concrete – a new processing route for architects and builders," *Mater. Des.*, vol. 100, pp. 102–109, Jun. 2016.
[6] S. Lim, R. A. Buswell, T. T. Le, S. A. Austin, A. G. F. Gibb, and T. Thorpe, "Developments in construction-scale additive manufacturing processes," *Autom. Constr.*, vol. 21, pp. 262–268, Jan. 2012.
[7] A. Kazemian, X. Yuan, E. Cochran, and B. Khoshnevis, "Cementitious materials for construction-scale 3D printing: Laboratory testing of fresh printing mixture," *Constr. Build. Mater.*, vol. 145, pp. 639–647, Aug. 2017.
[8] Y. W. Tay *et al.*, "Processing and Properties of Construction Materials for 3D Printing," *Materials Science Forum*, 2016. [Online]. Available: https://www.scientific.net/MSF.861.177. [Accessed: 20-Jul-2018].
[9] G. N. Levy, R. Schindel, and J. P. Kruth, "Rapid Manufacturing and Rapid Tooling With Layer Manufacturing (Lm) Technologies, State of the Art and Future Perspectives," *CIRP Ann.*, vol. 52, no. 2, pp. 589–609, Jan. 2003.
[10] A. S. Hanna, *Concrete Formwork Systems*. CRC Press, 1998.
[11] B. Khoshnevis and R. Dutton, "Innovative Rapid Prototyping Process Makes Large Sized, Smooth Surfaced Complex Shapes in a Wide Variety of Materials," *Mater. Technol.*, vol. 13, no. 2, pp. 53–56, Jan. 1998.
[12] F. Bos, R. Wolfs, Z. Ahmed, and T. Salet, "Additive manufacturing of concrete in construction: potentials and challenges of 3D concrete printing," *Virtual Phys. Prototyp.*, vol. 11, no. 3, pp. 209–225, Jul. 2016.
[13] L. Feng and L. Yuhong, "Study on the Status Quo and Problems of 3D Printed Buildings in China," p. 5, 2014.
[14] P. Feng, X. Meng, J.-F. Chen, and L. Ye, "Mechanical properties of structures 3D printed with cementitious powders," *Constr. Build. Mater.*, vol. 93, pp. 486–497, Sep. 2015.
[15] P. Shakor, J. Sanjayan, A. Nazari, and S. Nejadi, "Modified 3D printed powder to cement-based material and mechanical properties of cement scaffold used in 3D printing," *Constr. Build. Mater.*, vol. 138, pp. 398–409, May 2017.
[16] F. P. Glasser and L. Zhang, "High-performance cement matrices based on calcium sulfoaluminate–belite compositions," *Cem. Concr. Res.*, vol. 31, no. 12, pp. 1881–1886, Dec. 2001.
[17] C. Shi, A. F. Jiménez, and A. Palomo, "New cements for the 21st century: The pursuit of an alternative to Portland cement," *Cem. Concr. Res.*, vol. 41, no. 7, pp. 750–

763, Jul. 2011.
[18] ExOne, “https://www.exone.com/Systems/Production-Printers/Exerial.” .
[19] B. Utela, D. Storti, R. Anderson, and M. Ganter, “A review of process development steps for new material systems in three dimensional printing (3DP),” *J. Manuf. Process.*, vol. 10, no. 2, pp. 96–104, Jul. 2008.
[20] FairmountSantrol, “https://fairmountsantrol.com/wp-content/uploads/2014/09/FM-0558_Wedron_SilicaSand_Sheet.pdf.” .
[21] J. T. Fox *et al.*, “Waste Green Sand to Core Sand Reclamation, Demonstration via Casting Study, with Simultaneous Clay Recovery via a novel Ultrasonic-Cavitation System,” *AFS Transations*, vol. 140, pp. 523–538, 2008.
[22] ASTM International, “ASTM C128-15 Standard Test Method for Relative Density (Specific Gravity) and Absorption of Fine Aggregate.” ASTM International, West Conshohocken, PA, 2015.
[23] ASTM International, “ASTM C109/C109M-16a Standard Test Method for Compressive Strength of Hydraulic Cement Mortars (Using 2-in. or [50-mm] Cube Specimens).” ASTM International, West Conshohocken, PA, 2016.
[24] ASTM International, “ASTM C78/C78M-18 Standard Test Method for Flexural Strength of Concrete (Using Simple Beam with Third-Point Loading).” ASTM International, West Conshohocken, PA, 2018.
[25] American Foundry Society, *Mold & Core Test Handbook, Fourth Edition*. American Foundry Society, 2015.
[26] ACI Committee 318, *Building code requirements for structural concrete (ACI 318-14): an ACI standard : commentary on building code requirements for structural concrete (ACI 318R-14) : an ACI report*. Farmington Hills: American Concrete Institute, 2014.
[27] ACI Committee 209, *ACI 209R-92 Prediction of Creep, Shrinkage, and Temperature Effects in Concrete Structures*. Farmington Hills: American Concrete Institute, 1997.

AUTHOR BIOGRAPHY

Joseph P. Ingaglio was born in Scranton, Pennsylvania on September 21, 1993 to parents Raphael and Lisa Ingaglio. His family also includes an older brother, Raphael-Adrian Ingaglio II, a younger sister, Maria Ingaglio, and his fiancée Abby Winter. Joseph is a 2012 graduate of Western Wayne High School. He received his Bachelors of Science in Civil Engineering from Lehigh University in 2016. After graduating, he will remain at Lehigh to pursue a PhD in Structural Engineering.